



HAL
open science

Cables are elastic waveguides with granular cross section

Pierric Mora, Fabien Treyssède, Laurent Laguerre

► **To cite this version:**

Pierric Mora, Fabien Treyssède, Laurent Laguerre. Cables are elastic waveguides with granular cross section. 25ème Congrès Français de Mécanique, Aug 2022, Nantes, France. hal-03838633

HAL Id: hal-03838633

<https://hal.science/hal-03838633>

Submitted on 3 Nov 2022

HAL is a multi-disciplinary open access archive for the deposit and dissemination of scientific research documents, whether they are published or not. The documents may come from teaching and research institutions in France or abroad, or from public or private research centers.

L'archive ouverte pluridisciplinaire **HAL**, est destinée au dépôt et à la diffusion de documents scientifiques de niveau recherche, publiés ou non, émanant des établissements d'enseignement et de recherche français ou étrangers, des laboratoires publics ou privés.

Cables are elastic waveguides with granular cross section

P. Mora^{a,*}, F. Treyssède^a, L. Laguerre^a

a. GeoEND, GERS-GeoEND, Univ Gustave Eiffel, IFSTTAR, F-44344 Bouguenais, France

* pierric.mora@univ-eiffel.fr

Résumé :

Les câbles jouent bien souvent un rôle clé de répartition de la charge dans les ouvrages d'art. Les ondes mécaniques guidées peuvent être exploitées pour en sonder l'état de santé dans les zones faibles et détecter par exemple des ruptures de fils au voisinage d'un ancrage. Dans cette présentation, nous introduisons une nouvelle manière de modéliser la propagation des ondes élastiques dans un câble. L'exemple d'application choisi est le toron à sept brins qui est utilisé dans les câbles de précontrainte du génie civil. Nous nous inspirons des méthodes issues des milieux granulaires qui représentent à basse fréquence les grains comme des masses rigides et les contacts comme des ressorts, dont la raideur est donnée par la loi de Hertz. La spécificité du câble est que les contacts avec le brin central ne sont pas ponctuels, mais linéiques. Nous dérivons des nouvelles formules de raideurs longitudinales et transversales et montrons qu'elles permettent d'interpréter les premières fréquences de coupure comme des résonances de contact. Nous mettons également en évidence l'influence du phénomène de couplage non-local (entre seconds voisins), qui est spécifique au cas du contact linéique. Une comparaison avec un modèle aux éléments finis est donnée en fonction de la tension statique appliquée au câble, aux basses fréquences. Cette approche ouvre des perspectives pour la modélisation de la propagation dans les câbles multicouches, comportant un grand nombre de brins, tels que ceux utilisés comme haubans de ponts ou comme amarres d'éoliennes flottantes, et pour lesquels les approches par éléments finis 3D semblent à ce jour bien trop coûteuses pour pouvoir être appliquées.

Abstract :

Cables often play a key role in carrying loads in civil engineering structures. Guided mechanical waves offer a way to probe their health state in well chosen weak zones, and enable to detect e.g. broken wires near anchors. In this contribution we introduce a new way to model elastic wave propagation in cables. We apply the method to a seven-wire strand, which is a building element of prestressed cables. Our work is inspired by methods from the field of granular media which represent grains as rigid bodies and contacts as springs whose stiffness is given by Hertz law, in the quasi-static approximation. The specificity of cables is that contacts with the central wire are not point-wise, but line-wise. We derive new formulas of contact stiffness for normal and transverse line loads, and show that they enable to understand the lowest-order cutoff frequencies of the strand as contact resonances. We highlight the influence of non-local coupling (second neighbor coupling), which is absent for point contacts but appears here due to line contacts. A comparison with a finite element model is given at low frequencies, for several pre-stress states. This approach seems promising to model wave propagation in multilayer

cables – which are made of many wires – such as those used in cable-stayed bridges or to moor floating windmills to sea ground, and for which 3D finite elements remain today over-expensive.

Mots clefs : Guided waves, Seven-wire strand, Line contacts, Contact resonances, Discrete Element Method

1 Introduction

1.1 Context: Assessing the health state of civil engineering cables using mechanical guided waves

Mechanical guided waves can propagate over long distances in cables and be used to obtain information on possible damage. For instance, acoustic emission monitoring techniques are routinely deployed on cable-stayed bridges to track wire-break events [1]. Another example of a field technique is the inspection of anchors of prestressed cables using ultrasounds [2]. Let us also mention recent works that have explored the potentials of these waves to probe overhead transmission line cables [3], or the armor protecting submarine power cables [4].

The emergence of these monitoring and inspection techniques has motivated the study of how elastic waves propagate and attenuate in such complex assemblies: Wires are helical, they are kept in contact one another by a given pre-stress, and they often interact with a surrounding medium (cement grout, polymer matrix, water, ...). Modeling all these factors can be done within a framework of a Finite Elements representation of a unit cell. In the case of a seven-wire strand, the helical symmetry can be leveraged to reduce the mesh to the cross-section only while accounting analytically for harmonic on-axis propagation: this is the so-called Semi Analytical Finite Elements (SAFE) method [5, 7].

1.2 The “notch frequency” phenomenon

One noticeable achievement of SAFE has been to explain a long-standing mysterious effect called “notch frequency”, first reported by Kwun *et al.* [8]: In a transmit/receive wave propagation experiment using longitudinal transducers, these authors observed that a certain frequency was missing in the received spectrum. This notch frequency was furthermore found to depend on the tensile state of the strand as – roughly – the logarithm of the tension, and was not observed without applied tension. By representing each wire with Finite Elements, converting the applied tension into inter-wire normal pressure (Costello’s formulas), and connecting the meshes along contact areas (Hertz’s law), the notch frequency phenomenon and its dependence with tension could be reproduced numerically, and explained as the hybridization (curve veering effect) of the fundamental longitudinal mode with a higher order mode at its cutoff frequency [6, 7].

1.3 The issues, and our contributions

Finite-Elements-based modeling strategies are however demanding in computational resources. Indeed, as emphasized by the notch frequency phenomenon, contacts play an important role in dynamics and must be finely meshed. Today, except for highly symmetric geometries [4], it is by far prohibitively expensive to address cables made of many wires such as stays or mooring cables.

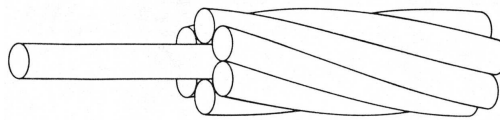


Figure 1: Scheme of a seven-wire strand used in prestressed cables.

How to design another strategy to broaden the applicability of numerical modeling to such many-wire-cables and support the development of novel monitoring methods?

Our starting guess is that the notch frequency could be understood more intuitively as a characteristic frequency of a masses-springs system. It would therefore be the signature that concepts employed to describe the mechanics of granular assemblies might be applied here to simplify the modeling and drastically reduce the computational burden in the quasi-statics approximation. To test this simple idea one has to know what spring constant values to take to build the stiffness matrix of the system. One then faces an unexpected bibliographic obstacle: Where can these formulas be found? Complete sets of formulas are available [9, 10] for non-conformal 3D Hertzian contacts involving solids of arbitrary shape. 2D geometries are notoriously far more difficult because the Green’s function (displacement field) of the half-space diverges at infinity as $\log r$, meaning that a local account of curvatures is not enough but must be replaced by an entire consideration of the shapes of the solids and of how they are supported. Still, as surprising as it might seem for such a canonical problem, the best one can find in the literature is the force-displacement relation for one cylinder pressed by two others [10]. In our case, this formula can provide good orders of magnitudes when only radial motions are involved, but do not accurately predict all radial effects (non-local coupling), and certainly cannot account for tangential coupling. On the way of deriving these missing relations, one faces another unexpected bibliographic obstacle: Where can the elastostatic Green’s functions of a cylinder be found? One of them, the response of “the heavy cylinder”, is a classic and is given in many textbooks – though usually only the stress field is given. The other two cases with tangential edge load and body balance are, to the best of our knowledge, not reported, even though all necessary pieces to build them are known since Michell’s article [11, 12].

After deriving new formulas for normal and tangential line contacts between cylinders, assembling the mass and stiffness matrices representing a seven-wire strand (see Fig. 1), and obtaining the normal modes (the eigenfrequencies of the strand at zero wavenumber), we show that the notch frequency is indeed a contact resonance. More generally, we show that 18 higher order modes start at cutoff frequencies that are contact resonances. Therefore, we propose this approach as a promising direction to solve the dispersion relations and compute the low-frequency response of cables made of many wires.

1.4 Inspiration and relation to other work

Cables are not often labeled as being part of the family of granular materials, but the idea is already mentioned in Roux’s work [13] among other examples illustrating force networks. More recently, although not speaking of a granular assembly, Argatov [14] derived appropriate contact stiffness formulas to account analytically for radial inter-wire contact deformation in a seven-wire strand. To our knowledge, his article is the only accessible report of the displacement¹ solution to the “heavy cylinder” problem – the cited source seems extremely difficult to find. A noticeable work inspired by Argatov’s article is due to Foti and Martinelli [15], also about radial contacts within the seven-wire strand.

¹Unfortunately, the formulas reported suffer from typo errors.

Another inspiring background are the many works that model wave propagation in granular packings in ways that relate to Cundall and Strack's Distinct (or Discrete) Element Method [16]. As a few samples, one may cite [17] and [18] which deal with cylinders. These works and the others in the literature however deal with formulas for contact stiffnesses that bound only particles in contact, and as such neglect part of the underlying equations of mechanics (although they probably do capture most of the physical phenomena which they discuss). In essence, except for aspects that are specific to line contacts that are derived here starting from Green's formulas and Hertz law with the aim to compete with a Finite Elements calculation, our modeling scheme also follows the path shown by Cundall and Strack.

2 Theory: Adapting the Discrete Element Method to assemblies of cylinders in Hertzian contact

We start by recalling how the forced response of a single wire can be decomposed into a global, rigid-body motion (the skeleton), plus a field which accounts for the elastic deformation due to the application of the load (inner displacement). Then, the principle of the Discrete Element Method is to convert the inner field into spring constants that connect the skeleton to its neighbors and thus to reduce the state vector of the system to 4 degrees of freedom per wire (3 translations and 1 rotation): We show how to adapt this method to assemblies of cylinders by taking the seven-wire strand as case study. We recall only briefly the main steps, with an emphasis on important formulas (gauges, force-displacement relations for line contacts) that are new or less known. Detailed derivations and discussions will be given in forthcoming articles [19, 20].

2.1 Forced motion of a single wire

In this part we neglect curvature effects: we assume that peripheral wires are straight cylinders, and that contacts with the central wire are along straight lines. Furthermore, we limit ourselves to fields that are invariant along the axis (zero wavenumber, *i.e.* infinite wavelength).

We call R the radius of a cylinder, ρ its density, μ its shear modulus, and ν its Poisson's ratio.

2.1.1 Balance of forces, skeleton, and inner displacement

Let us call $\mathbf{U}_{tot}(\mathbf{r}) = (U_{tot,x}, U_{tot,y}, U_{tot,z})^T$ the displacement field of the wire under consideration relative to a known static state, where $\mathbf{r} = (x, y)^T$ refers to the distance to the axis of the cylinder in that static state. \mathbf{U}_{tot} is caused by a set of forces \mathbf{F}_j which represent Hertzian contacts with neighboring wires and is assumed to be small. \mathbf{F}_j are actually distributed along small contact lengths; by \mathbf{F}_j we may equally refer to the distribution or to its average value, for convenience.

We expand \mathbf{U}_{tot} as follows:

$$\mathbf{U}_{tot} = \mathbf{U} + \boldsymbol{\theta} \times \mathbf{r} + \mathbf{u}. \quad (1)$$

- $\mathbf{U} + \boldsymbol{\theta} \times \mathbf{r}$ is the motion of the skeleton: \mathbf{U} is a uniform translation, and $\boldsymbol{\theta} \times \mathbf{r} = \theta \mathbf{e}_z \times \mathbf{r}$ is a uniform rotation.
- $\mathbf{u}(\mathbf{r})$ is an elastic displacement relative to the skeleton and is called "inner" field.

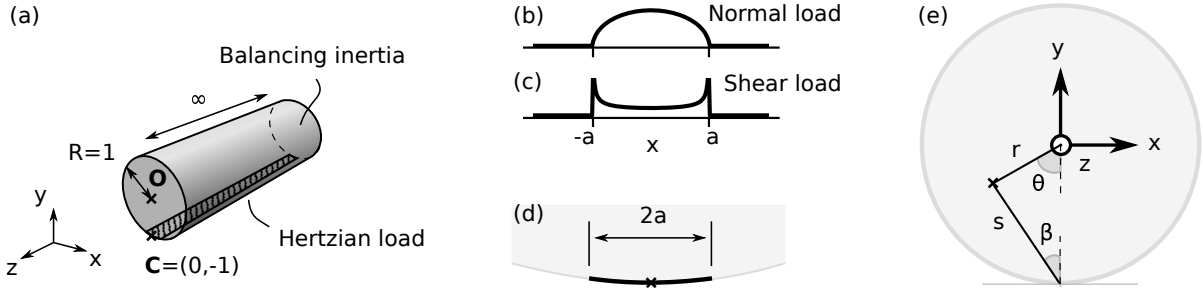


Figure 2: The elementary problem: A single wire loaded by a pressure distribution representative of a Hertzian contact (no slip) with a neighboring wire – the curvature is neglected. The static equilibrium is ensured by a force distribution proportional to the rigid-body motions.

To be uniquely defined, Expansion (1) requires to set four gauges on \mathbf{u} . We choose:

$$\iint_S \rho \mathbf{u} dS = 0, \quad (2a)$$

$$\iint_S \rho \mathbf{r} \times \mathbf{u} dS = 0, \quad (2b)$$

where the surface integrals relate to the cross-section of the cylinder. After differentiation with respect to time, and by keeping only first order terms, Gauges (2a) and (2b) average to zero linear and angular momentum for \mathbf{u} with respect to the center of mass. It then follows that the equations of motion of the skeleton take a simple form without explicit reference to \mathbf{u} :

$$m\ddot{\mathbf{U}} = \sum \mathbf{F}_j, \quad (3a)$$

$$J\ddot{\boldsymbol{\theta}} = \sum \mathbf{M}_j, \quad (3b)$$

with $m = \iint_S \rho dS = \rho\pi R^2$ the mass, $J = \iint_S \rho r^2 dS = \frac{1}{2}mR^2$ the moment of inertia about the principal axis, $\mathbf{M}_j = R \mathbf{n}_j \times \mathbf{F}_j$ the torque of \mathbf{F}_j about that same axis, and \mathbf{n}_j an outward normal unit vector at the point of application of \mathbf{F}_j .

2.1.2 Derivation of contact stiffness formulas between parallel cylinders in line contact

To establish the equations satisfied by \mathbf{u} without explicit reference to the motion of the skeleton, one can start from the equations of motion on \mathbf{U} , use Expansion (1), and then express the inertia of the skeleton in terms of the average loads using Eqs (3). Then, the static limit is taken by neglecting the inertia of \mathbf{u} compared to elastic terms. At this point it becomes convenient to express the problem as a superposition of three elementary problems that are represented in Fig. 2 and described in the next paragraph.

The three elementary problems: Without changing the notations, we now switch to a dimensionless coordinate system in which $R = 1$. We first search the displacement field \mathbf{u} of a cylinder loaded by a concentrated load applied on its edge $\mathbf{F} = \delta(\mathbf{r} - \mathbf{C})\mathbf{e}_i$, maintained in equilibrium by bulk forces that are proportional to the rigid-body motions of the cylinder $\mathbf{B} = B^T \mathbf{e}_i + B^R r \mathbf{e}_\theta$, with $B^T = -1/\pi$, $B^R = -2/\pi$ if $i = x$ and 0 otherwise, and satisfying the gauges (2). The three distinct cases are:

- $\mathbf{e}_i = \mathbf{e}_y$: normal load,

- $\mathbf{e}_i = \mathbf{e}_x$: in-plane tangential load,
- $\mathbf{e}_i = \mathbf{e}_z$: out-of-plane tangential load.

The solutions can be constructed by superposing the Flamant solution (Green's function of a half space), the uniform body force $B^T \mathbf{e}_i$, a rotational acceleration $B^R r \mathbf{e}_\theta$, additional terms among Michell's solutions to the biharmonic equation [11, 12] chosen to satisfy the free boundary condition, and rigid-body movements chosen to satisfy the gauges. The case of out-of-plane tangential load is simpler and can also be solved in a tractable manner by separation of variables. Then, these Green's functions are convolved by Hertzian distributions applied along a short segment of width $2a \ll 1$. For now a is an arbitrary parameter, its value will eventually be set according to Hertz's law. The distributions are:

- for the normal load, by calling P the average value:

$$F_y(x) = \frac{2P}{\pi a} \sqrt{1 - x^2/a^2} \quad \text{on } -a < x < a, \quad (4a)$$

$$= 0 \quad \text{elsewhere,} \quad (4b)$$

- for in-plane and out-of-plane tangential loads, by calling Q_x or Q_z the average value:

$$F_{x,z}(x) = \frac{Q_{x,z}}{\pi a} \frac{1}{\sqrt{1 - x^2/a^2}} \quad \text{on } -a < x < a, \quad (5a)$$

$$= 0 \quad \text{elsewhere.} \quad (5b)$$

Here the acoustic limit is taken by assuming full stick, as the divergence at the edges necessarily overpasses the slip limit and is then non-physical: this slip region is assumed to be infinitesimal.

The solutions to the elementary problems: The solutions are expressed using Kolosov's constant κ , which for plane strain² reads $\kappa = 3 - 4\nu$. We use two sets of polar coordinates: (r, θ) and (s, β) (see Fig.2-e). The convolutions are calculated analytically at the mid-point of application of the distributions (point C), and far from the load for $s \gg a$ by merely multiplying the Green's function by the load magnitude. The intermediate region $s \sim a$ is small and therefore not of interest.

- For the **normal load**, far from the load:

$$\frac{4\pi\mu}{P} u_x = -\sin 2\beta + (\kappa - 1)\beta + \frac{1}{2}(\kappa - 1)r \sin \theta + \frac{1}{2}r^2 \sin 2\theta, \quad (6a)$$

$$\frac{4\pi\mu}{P} u_y = -(\kappa + 1) \log s - 2 \sin^2 \beta - \frac{1}{2}(\kappa - 1)r \cos \theta + \frac{1}{2}r^2(1 + 2 \sin^2 \theta), \quad (6b)$$

and at the center of application of the load:

$$u_x(\mathbf{C}) = 0, \quad (7a)$$

$$\frac{4\pi\mu}{P} u_y(\mathbf{C}) = (\kappa + 1) \log \frac{2}{a} - \frac{1}{2}. \quad (7b)$$

²The formulas are also valid for plane stress (*i.e.* for thin disks) by taking $\kappa = (3 - \nu)/(1 + \nu)$.

- For the **in-plane tangential load**, far from the load:

$$\frac{4\pi\mu}{Q_x}u_x = -(\kappa + 1)\log s + 2\sin^2\beta + \frac{1}{2}r^2(1 + 2\cos^2\theta) + (r^3 - (\kappa + \frac{5}{3})r)\cos\theta - 1, \quad (8a)$$

$$\frac{4\pi\mu}{Q_x}u_y = -\sin 2\beta - (\kappa - 1)\beta + \frac{1}{2}r^2\sin 2\theta + (r^3 - (\kappa + \frac{5}{3})r)\sin\theta, \quad (8b)$$

and at the center of application of the load:

$$\frac{4\pi\mu}{Q_x}u_x(\mathbf{C}) = (\kappa + 1)\log \frac{2}{ae} + 3 - \frac{1}{6}, \quad (9a)$$

$$u_y(\mathbf{C}) = 0. \quad (9b)$$

- For the **out-of-plane tangential load**, far from the load:

$$\frac{4\pi\mu}{Q_z}u_z = -4\log s + r^2 - \frac{1}{2}, \quad (10)$$

and at the center of application of the load:

$$\frac{4\pi\mu}{Q_z}u_z(\mathbf{C}) = 4\log \frac{2}{a} + \frac{1}{2}. \quad (11)$$

These solutions are represented in Fig. 3. They constitute force-displacement relations from which, by differentiation, one obtains compliance constants. Note that because $a = a(P)$ is actually a function of the normal pressure (by Hertz law), the compliance is calculated around a given static state.

2.2 Free motion of the cable

In this part we construct the mass and stiffness matrices of the system, and obtain the normal modes.

2.2.1 Contacts within the seven-wire strand

Each contact will be expressed by demanding continuity on the displacement \mathbf{U}_{tot} and the stress. Our model for the seven-wire strand is that contacts occur only between peripheral wires and the core wire, *i.e.* peripheral-to-peripheral contacts are excluded. This model is supported by the fact that the radii are such that, theoretically, there is a small gap between neighboring peripheral wires [21, 22], that this gap is furthermore made wider by Poisson effect when tension is applied to the strand, and that post-mortem observations of strands after tensile tests show clear plastic flow at peripheral-to-core contacts and no track of peripheral-to-peripheral contact.

2.2.2 Inter-wire pressure and contact width for a given tensile state

Due to the helical geometry of peripheral wires, applying a static tension to the strand compresses the peripheral wires to the core. Let us call P this normal pressure. Costello's formulas [23] result in a

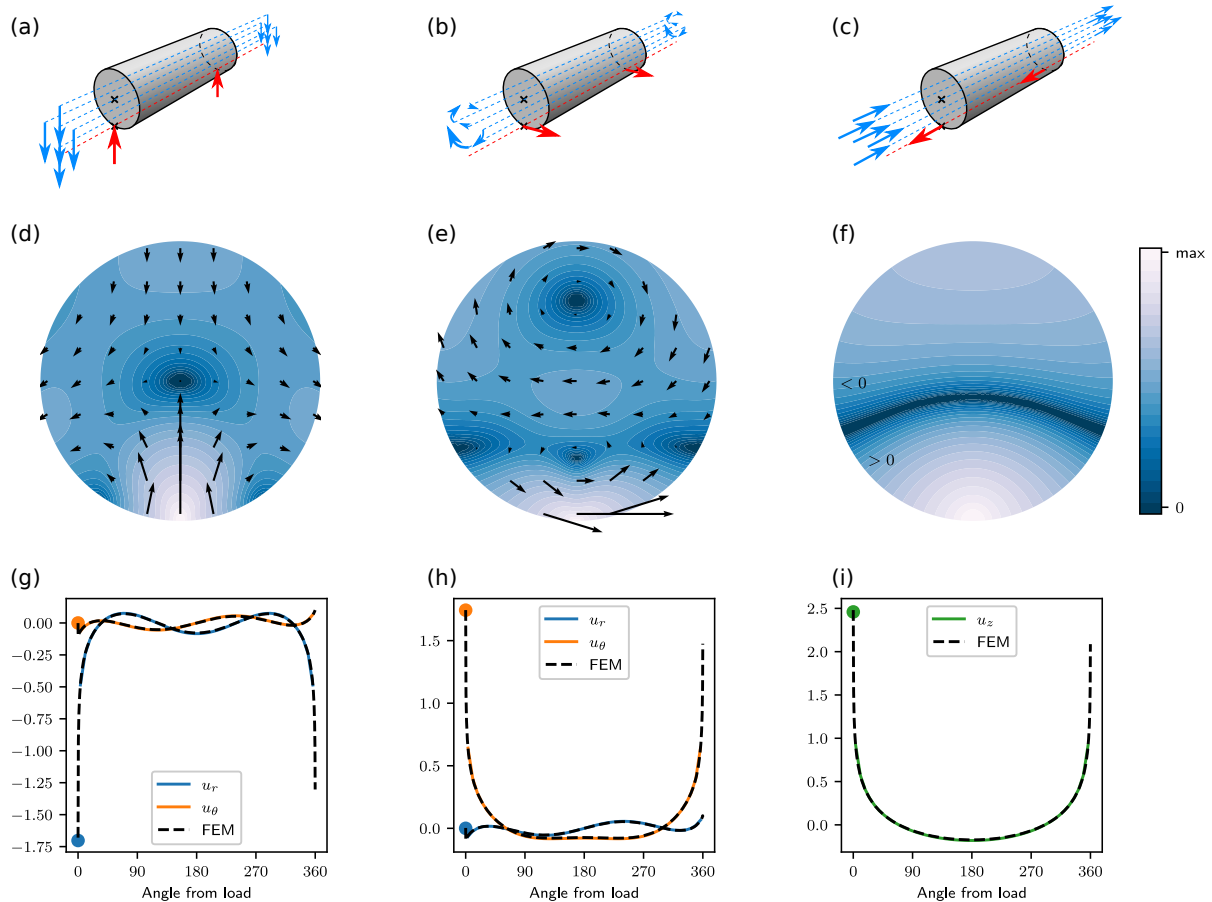


Figure 3: Analytical solutions to the three static elementary problems. (a), (b) and (c): Schemes of the load distributions. (d), (e) and (f): Full field – log scale colors are proportional to the magnitude of the displacement. (g), (h) and (i): Response at the edge, validated with a Finite Elements computation (dashed lines). Solid lines: solution far from the load. Dots: solution at the center of application of the load. Parameters : $\nu = 0.28$ (Poisson's ratio of steel), $P, Q_x, Q_z = \mu$ (load magnitude set to shear modulus), Hertzian load of half-width $a = 0.1\%$.

relation of the form:

$$P = A\epsilon, \quad (12)$$

with ϵ the applied longitudinal strain and A a constant which depends on the elasticity and geometry of the wires. Once P is known, the contact half-widths can be calculated from [10]:

$$a = \sqrt{\frac{4PR^*}{\pi E^*}}, \quad (13)$$

with $R^* = (R_c^{-1} + R_p^{-1})^{-1}$ and $E^* = E/2(1 - \nu^2)$. We can now differentiate the force-displacement relations (6) to (11) around the static state defined by P .

2.2.3 Mass and stiffness matrices of the system

We here start by describing in details the steps to obtain the system of equations on the out-of-plane degrees of freedom. The procedure for in-plane motions is similar.

Global reference frame, and labeling: We label the core wire with index $i = 0$ (radius: R_c) and peripheral wires with indexes $i = 1..6$ (radii: R_p). We define a coordinate system whose origin coincides with the center of the core at rest, and in which the center of the peripheral wire i is at $(R_c + R_p)\mathbf{n}_i$, with $\mathbf{n}_i = (\cos((i-1)\pi/3), \sin((i-1)\pi/3))^T$. The contact points are at $\mathbf{C}_i = R_c\mathbf{n}_i$.

Inner displacements, compliance matrix: Let us call:

$$\boldsymbol{\delta}_z = [u_z^{(0)}(\mathbf{C}_i) - u_z^{(i)}(\mathbf{C}_i)]_{1 \leq i \leq 6} \quad (14)$$

the state vector containing the total inner displacements at the points of contact. We also call $\mathbf{F}_z = [F_z^{i \rightarrow 0}]_{1 \leq i \leq 6}$ the vector containing the forces acting on the core wire and applied at \mathbf{C}_i . By using Eqs. (10) and (11), and that $F_z^{0 \rightarrow i} = -F_z^{i \rightarrow 0}$, contact forces and inner displacements relate as:

$$\boldsymbol{\delta}_z = \mathbf{C}_z \mathbf{F}_z, \quad (15)$$

where $\mathbf{C}_z(a)$ is the compliant matrix whose components are (remember that Eqs. (10) and (11) are defined with dimensionless coordinates):

$$4\pi\mu\mathbf{C}_{z,ij} = \begin{cases} 4 \log \frac{2R_c}{a} + 4 \log \frac{2R_p}{a} + 1, & i = j, \\ 1 - 2 \log \left(2 - 2 \cos \frac{(i-j)\pi}{3} \right), & i \neq j. \end{cases} \quad (16)$$

The elastic energy expresses as:

$$\mathcal{V}_z = \frac{1}{2} \boldsymbol{\delta}_z^T \mathbf{C}_z^{-1} \boldsymbol{\delta}_z. \quad (17)$$

Skeleton motion: Let us call:

$$\mathbf{U}_z = [U_z^{(i)}]_{0 \leq i \leq 6} \quad (18)$$

the state vector containing the degrees of freedom of the skeleton. Remembering Eq. (1), continuity at contacts expresses as $\delta_z^{(i)} = -(U_z^{(0)} - U_z^{(i)})$. By defining $\mathbf{D}_z = -[\delta_{0,j} - \delta_{i,j+1}]_{i,j}$ a 6×7 matrix, where

$\delta_{i,j}$ is the Kronecker delta, continuity reads:

$$\boldsymbol{\delta}_z = \mathbf{D}_z \mathbf{U}_z. \quad (19)$$

The elastic energy in Eq. (17) then reads:

$$\mathcal{V}_z = \frac{1}{2} \mathbf{U}_z^T \boldsymbol{\mathcal{K}}_z \mathbf{U}_z, \quad (20)$$

in which $\boldsymbol{\mathcal{K}}_z = \mathbf{D}_z^T \mathbf{C}_z^{-1} \mathbf{D}_z$ is the stiffness matrix. On the other hand, the kinetic energy expresses as:

$$\mathcal{T}_z = \frac{1}{2} \mathbf{U}_z^T \boldsymbol{\mathcal{M}}_z \mathbf{U}_z, \quad (21)$$

with $\boldsymbol{\mathcal{M}}_z = \text{diag}\{[m_i]_{0 \leq i \leq 6}\}$ and m_i the mass of wire i .

In-plane motion: The above steps are similar for in-plane degrees of freedom. It is convenient to use polar coordinates to relate inner displacements and forces at contacts. We define:

$$\boldsymbol{\delta}_{xy} = [u_r^{(0)}(\mathbf{C}_i) - u_r^{(i)}(\mathbf{C}_i), u_\theta^{(0)}(\mathbf{C}_i) - u_\theta^{(i)}(\mathbf{C}_i)]_{1 \leq i \leq 6}, \quad (22)$$

and $\mathbf{F}_{xy} = [F_r^{i \rightarrow 0}, F_\theta^{i \rightarrow 0}]_{1 \leq i \leq 6}$. After differentiation, Eqs. (6) to (9) can be assembled into:

$$\boldsymbol{\delta}_{xy} = \mathbf{C}_{xy} \mathbf{F}_{xy}, \quad (23)$$

where $\mathbf{C}_{xy}(a)$ is the compliant matrix. Note that the dependence of the contact half width on pressure (Eq. (13)) also has to be differentiated and enters into account in the diagonal terms of \mathbf{C}_{xy} involving $u_r^{(0)}(\mathbf{C}_i) - u_r^{(i)}(\mathbf{C}_i)$ and $F_r^{i \rightarrow 0}$ (even indexes):

$$\mathcal{C}_{xy,2i,2i} = \frac{\partial u_r^{(0)}(\mathbf{C}_i)}{\partial F_r^{i \rightarrow 0}} + \frac{\partial u_r^{(i)}(\mathbf{C}_i)}{\partial F_r^{0 \rightarrow i}}, \quad (24a)$$

$$4\pi\mu\mathcal{C}_{xy,2i,2i} = (\kappa + 1) \left(\log \frac{2R_c}{a} + \log \frac{2R_p}{a} - \frac{1}{2} - \frac{1}{2} \right) - \frac{1}{2} - \frac{1}{2}. \quad (24b)$$

$$4\pi\mu\mathcal{C}_{xy,2i+1,2i+1} = (\kappa + 1) \left(\log \frac{2R_c}{ae} + \log \frac{2R_p}{ae} \right) + 6 - \frac{1}{3}. \quad (25)$$

Off-diagonal terms $i \neq j$ are obtained using Eqs. (6) and (8) transformed into polar coordinates:

$$\mathcal{C}_{xy,2i,2j} = \partial u_r^{(0)}(\mathbf{C}_i) / \partial F_r^{j \rightarrow 0}, \quad (26)$$

$$\mathcal{C}_{xy,2i,2j+1} = \partial u_r^{(0)}(\mathbf{C}_i) / \partial F_\theta^{j \rightarrow 0}, \quad (27)$$

$$\mathcal{C}_{xy,2i+1,2j} = \partial u_\theta^{(0)}(\mathbf{C}_i) / \partial F_r^{j \rightarrow 0}, \quad (28)$$

$$\mathcal{C}_{xy,2i+1,2j+1} = \partial u_\theta^{(0)}(\mathbf{C}_i) / \partial F_\theta^{j \rightarrow 0}. \quad (29)$$

We define the state vector of the skeleton as:

$$\mathbf{U}_{xy} = [U_x^{(i)}, U_y^{(i)}, \theta^{(i)}]_{0 \leq i \leq 6}. \quad (30)$$

Continuity at contacts expresses as $\delta_{xy}^{(2i)} = -\mathbf{n}_i^T (\mathbf{U}^{(0)} - \mathbf{U}^{(i)})$, $\delta_{xy}^{(2i+1)} = -\mathbf{t}_i^T (\mathbf{U}^{(0)} - \mathbf{U}^{(i)}) - (R_c \theta^{(0)} - R_p \theta^{(i)})$, with $\mathbf{t}_i = \mathbf{e}_z \times \mathbf{n}_i$ a tangential unit vector at point \mathbf{C}_i . These continuity relations are assembled in a 12×21 matrix \mathbf{D}_{xy} , such that:

$$\boldsymbol{\delta}_{xy} = \mathbf{D}_{xy} \mathbf{U}_{xy}. \quad (31)$$

The elastic energy reads:

$$\mathcal{V}_{xy} = \frac{1}{2} \mathbf{U}_{xy}^T \mathcal{K}_{xy} \mathbf{U}_{xy}, \quad (32)$$

where $\mathcal{K}_{xy} = \mathbf{D}_{xy}^T \mathcal{C}_{xy}^{-1} \mathbf{D}_{xy}$ is the stiffness matrix, while the kinetic energy

$$\mathcal{T}_{xy} = \frac{1}{2} \mathbf{U}_{xy}^T \mathcal{M}_{xy} \mathbf{U}_{xy} \quad (33)$$

gives the expression of the mass matrix $\mathcal{M}_{xy} = \text{diag}\{[m_i, m_i, J_i]_{0 \leq i \leq 6}\}$, with J_i the moment of inertia of wire i about its axis.

2.2.4 Normal modes

Finally, the normal modes of the cable are obtained by solving the following generalized eigenvalue problem:

$$\mathcal{K} \mathbf{U}_n = \omega_n^2 \mathcal{M} \mathbf{U}_n, \quad (34)$$

where $(\mathcal{M}, \mathcal{K})$ stand for either $(\mathcal{M}_z, \mathcal{K}_z)$ or $(\mathcal{M}_{xy}, \mathcal{K}_{xy})$. There are 7 modes with z polarization, among which 1 rigid-body translation, and 21 modes with xy polarization, among which 2 rigid-body translations and 7 rigid-body rotations. In total, there are 18 non-trivial modes.

3 Numerical results

We now present a numerical application of the above equations to a “T15.7” steel strand.

3.1 Parameters

The parameters are set to:

- Material (steel): $\rho = 7800 \text{ kg/m}^3$, $E = 217 \text{ GPa}$ (Young’s modulus), $\nu = 0.28$.
- Sizes: $R_c = 2.7 \text{ mm}$ (radius of the core), $R_p = 0.967 R_c$ (radius of peripheral wires).
- Helix: $\phi = 7.9^\circ$ (lay angle).
- Static state: ϵ (applied strain) is varied up to 0.6% which corresponds to an in-service state.

With these parameters, Costello’s formulas give a value of $A \approx 1.60 \times 10^7 \text{ N/m}$ that relates the applied strain to peripheral-to-core normal pressure (see Eq. (12)).

In order to compare the results obtained with the Discrete Element Method detailed here, a Finite Elements model is build (SAFE method, see Introduction) which fully takes into account curvature effects through a system of coordinates that leverages the helical symmetry. Details on this SAFE formulation can be found in [5]. The mesh used consists of 5673 nodes.

The results are represented in Figs. 4 and 5.

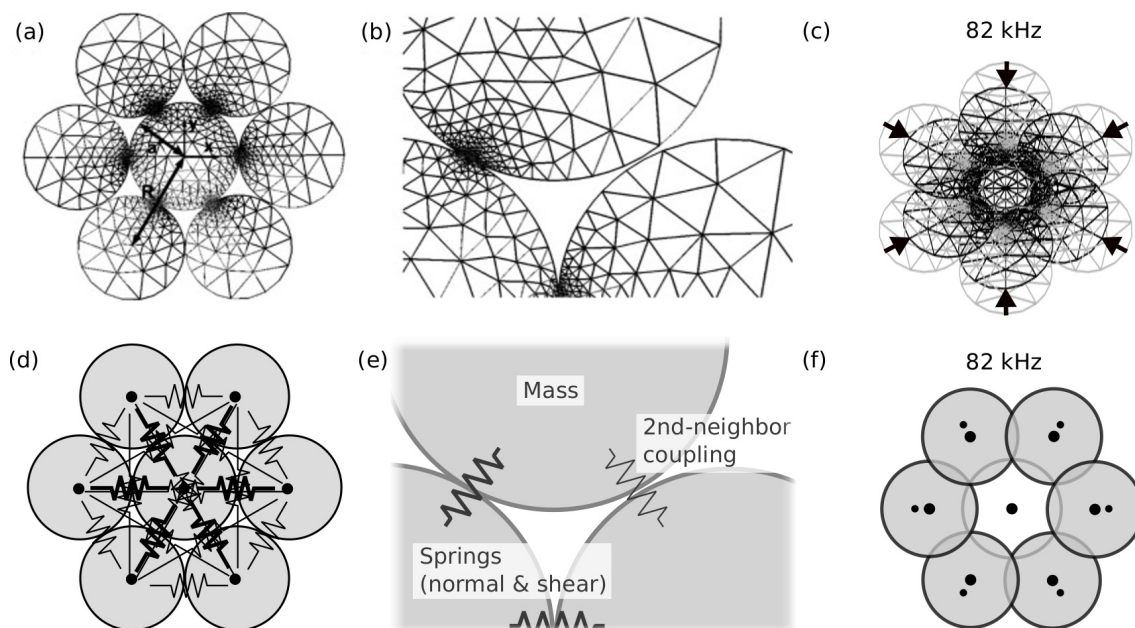


Figure 4: Finite Elements versus Discrete Elements representations of a seven-wire strand. (c) and (f): The normal mode responsible for the “notch frequency” phenomenon for an applied strain of $\epsilon = 0.6\%$. (d) and (e): In contrast to the intuitive case of contacts between spheres or 3D shapes that are represented with local springs, 2nd neighbors are here directly coupled with non-zero spring constants as a result of line contacts. (a) and (b) adapted from [5].

3.2 Discussion

Figure 5 shows a very good quantitative agreement – except for the second last eigenfrequency: the reason of this discrepancy is currently not understood. This match confirms that the approximations made (quasi-static assumption, and neglecting curvature effects in the contact stiffnesses) are relevant to obtain the first higher order modes of the strand while drastically lowering the numerical costs. It also provides a simplified understanding of these modes as the concept of contact resonance is well suited to interpret their cutoff frequencies. Among those resonances is the mode that is responsible for the notch frequency phenomenon observed by Kwun *et al.* [8] (see Introduction): it is part of the set of the lowest resonances that have in-plane polarization. The polarization of this mode is represented in Figs. 4-(c) and 4-(f): all peripheral wires have a purely radial motion and are in-phase while the core remains still. The modes having slightly different eigenfrequencies have similar polarizations, but with different phase relations between peripheral wires.

The main specificity of this adaptation of the Discrete Element Method to cylinders in line contact is that the stiffness matrix is dense, *i.e.* direct coupling is not limited to direct contacts but also relate 2nd neighbors with non-zero spring constants (depicted in Figs 4-(d) and -(e)). As recalled in the Introduction, this fact is a direct consequence of the long-range behavior of the Green’s function of the half-space: in 2D, the displacement field diverges at infinity while it tends to 0 in 3D. This non-zero cross-influence can be seen on the Green’s functions of the cylinder represented in Figs. 3-(g), -(h), -(i): although substantially smaller than at the contact point, the response is not negligible on the entire border. In other words, compressing the core cylinder with peripheral cylinders does not result in the same apparent contact stiffness depending on whether the peripheral cylinders are in-phase or not. A consequence of this non-local coupling is that the multiplicity of eigenvalues is smaller than intuitively

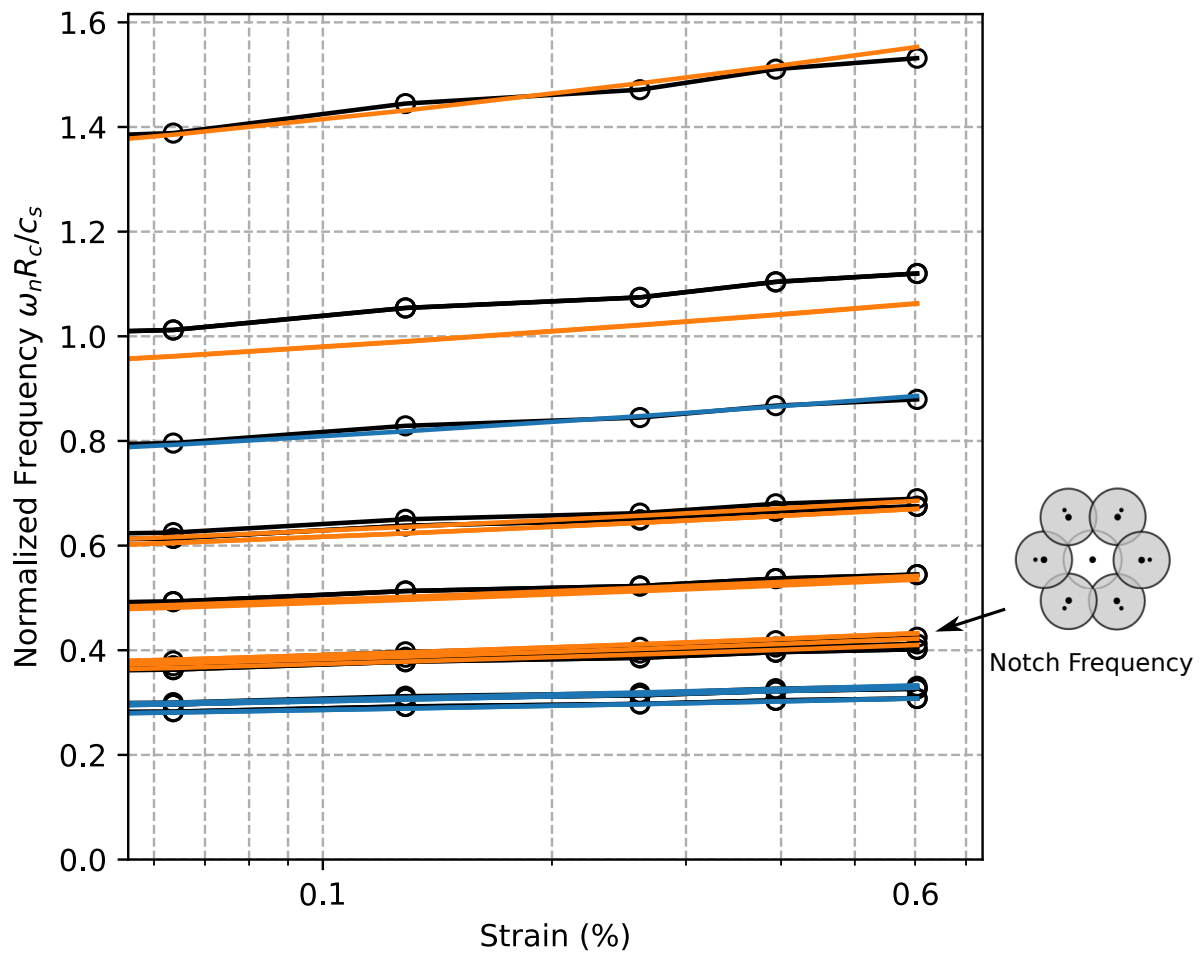


Figure 5: The 18 non-trivial eigenfrequencies of the seven-wire strand as a function of applied strain, compared with Finite Elements (circles). Orange / blue lines: modes with in-plane / out-of-plane polarization.

expected for only 1st neighbor coupling. This can be seen in Fig. 5 for *e.g.* the lowest resonances with in-plane polarization (orange lines): instead of one eigenfrequency of multiplicity 4, there are 3 distinct eigenfrequencies (the lowest of which being of multiplicity 2, and the highest being the notch frequency).

4 Conclusion

The modeling scheme presented in this work seems full of promises to tackle cases that are currently out of reach with Finite Elements. The seven-wire strand was chosen as a case study to test the relevance of the hypotheses without adding unnecessary complexity, and to easily allow a comparison against a well established Finite Elements model. Despite that this case has been widely studied before, applying concepts from the field of granular materials brought new physical insights that will undoubtedly apply more generally to other cables.

The next step is to allow a harmonic axial dependence to solve the full dispersion relations and conduct a deeper analysis of the range of validity of the method. The seven-wire strand can however only serve as an easy-to-build playground as on-field inspections [2] rely on high frequencies, *i.e.* where this granular representation is irrelevant and where the SAFE method [5] remains the best modeling choice. As for now, we believe that the best opportunities of application of this approach are multi-layer civil engineering cables such as stays or mooring cables.

Acknowledgments

We thank Marc Bonnet (CNRS, POems team) and Patrice Cartraud (École Centrale de Nantes, GeM lab.) for stimulating discussions.

References

- [1] A. Nair and C.S. Cai, Acoustic emission monitoring of bridges: Review and case studies. *Engineering Structures*, 32 (2010), 1704-1714
- [2] L. Laguerre, O. Durand, and R. Colin, 27 oct. 2020, Method for detecting a defect in a metal wire of a set of metal wires, in particular for an anchoring area of a civil engineering structure. U.S. Patent No 10,816,511
- [3] M.K. Yücel, M. Legg, V. Kappatos, T.-H. Gan, An ultrasonic guided wave approach for the inspection of overhead transmission line cables, *Applied Acoustics* 122 (2017), 23-34
- [4] F. Treyssède, L. Laguerre, P. Cartraud, and T. Soulard, Elastic guided waves in helical multi-wire armors, *Ultrasonics* 110 (2021), 106294
- [5] F. Treyssède, A. Frikha, P. Cartraud, Mechanical modeling of helical structures accounting for translational invariance. Part 2: Guided wave propagation under axial loads, *International Journal of Solids and Structures*, 50 (2013), 1383–1393
- [6] F. Treyssède and L. Laguerre, Investigation of elastic modes propagating in multi-wire helical waveguides, *Journal of Sound and Vibration*, 329 (2010), 1702-1716

- [7] F. Treyssède, Dispersion curve veering of longitudinal guided waves propagating inside prestressed seven-wire strands, *Journal of Sound and Vibration*, 367 (2016), 56-68
- [8] H. Kwun, K.A. Bartels, J.J. Hanley, Effects of tensile loading on the properties of elastic-wave propagation in a strand, *Journal of the Acoustical Society of America*, 103 (1998), pp. 3370-3375
- [9] R.D. Mindlin, Compliance of Elastic Bodies in Contact, *Journal of Applied Mechanics*, 16 (1949), 259-268
- [10] K.L. Johnson, *Contact Mechanics*, Cambridge University Press, Cambridge, 1987
- [11] J.H. Michell, On the direct determination of stress in an elastic solid, with application to the theory of plates, *Proceedings of the London Mathematical Society*, Vol. 31 (1899), pp. 100–124.
- [12] J.R. Barber, *Elasticity*, 3rd Ed., Kluwer Academic Publishers, 2010
- [13] J.-N. Roux, Geometric origin of mechanical properties of granular materials, *Physical Review E*, 61 (2000), 6802-6836
- [14] I. Argatov, Response of a wire rope strand to axial and torsional loads: asymptotic modeling of the effect of interwire contact deformations, *International Journal of Solids and Structures*, 48 (2011), pp. 1413-1423
- [15] F. Foti and L. Martinelli, Modeling the axial-torsional response of metallic strands accounting for the deformability of the internal contact surfaces: Derivation of the symmetric stiffness matrix, *International Journal of Solids and Structures*, 171 (2019), 30-46
- [16] P.A. Cundall and O.D.L. Strack, A discrete numerical model for granular assemblies, *Géotechnique*, 29 (1979), 47-65
- [17] G. Huillard, X. Noblin, and J. Rajchenbach, Propagation of acoustic waves in a one-dimensional array of noncohesive cylinders, *Physical Review E*, 84 (2011), 016602
- [18] H. Pichard, A. Duclos, J.-P. Groby, V. Tournat, and V. E. Gusev, Two-dimensional discrete granular phononic crystal for shear wave control, *Physical Review B*, 86 (2012), 134307
- [19] P. Mora, F. Treyssède, and L. Laguerre, Elastic response of a cylinder loaded by a Hertzian contact pressure and maintained in equilibrium by its inertia. [In preparation]
- [20] P. Mora, F. Treyssède, and L. Laguerre, Contact stiffnesses between elastic cylinders. [In preparation]
- [21] A. Nawrocki, A finite element model for simple straight wire rope strands, *Computers and Structures*, 77 (2000), 345-359
- [22] F. Foti, A. de Luca di Roseto, Analytical and finite element modelling of the elastic-plastic behaviour of metallic strands under axial-torsional loads, *International Journal of Mechanical Sciences*, 115-116 (2016), 202-214
- [23] G. A. Costello, *Theory of wire ropes*, Springer-Verlag, New York, 1990